Peer-reviewed version available at *Appl. Sci.* **2020**, *10*, 3460; doi:10.3390/app10103460

Article

Optimal Design of a Plenum Fan with Three-Dimensional Blades

Kyung Jung Lee [1], Il Wung Park [1], Ki Suk Bang [1], Yeong Min Kim [1], Young-Chull Ahn [2,*]

[1] LG electronics, Changwon 2nd Factory, Seonsan-dong, Changwon-city, Keongsang Namdo 51554, Korea; kyungjung.lee@lge.com (K.J.L.); ilwung.park@lge.com (I.W.P.); gojang77.bang@lge.com (K.S.B.); Yeong.kim@lge.com (Y.M.K.)

[2] School of Architectural Engineering, Pusan National University, Busan 46241, Korea; ycahn@pusan.ac.kr (Y.C.A.)

* Correspondence: ycahn@pusan.ac.kr

Abstract: We successfully designed an optimized plenum fan with a three-dimensional, smooth, curved blade. The optimized model revealed that the static pressure in the channel had been increased uniformly and stably, and the flow separation at the leading edge was significantly reduced. To conclude, the three-dimensional blade stabilized the fluid flow, and the flow friction was reduced by suppressing the flow separation as much as possible so that both the static pressure and the static efficiency were clearly improved in comparison with those of the original model. The static efficiency, as a result, was improved by 6% compared with that of the original model.

Keywords: Plenum fan; Blade profile; Static pressure; Static efficiency; Velocity distribution; Pressure distribution

1. Introduction

Centrifugal fans are commonly used for industrial purposes or air-conditioning because they are more efficient and quieter than other fans at the same RPM(revolution per minute). Specifically, the plenum fan is quiet and small, it produces excellent airflow compared with existing centrifugal fans since it has no housing, and it is widely used for air-conditioning and ventilation.

In industrial use or air-conditioning, a fan's air-conveying power uses the majority of the energy consumption. Therefore, to reduce energy consumption and promote efficient use, the most important factor is to improve fan efficiency. The blade, the impeller of the centrifugal fan, is the most crucial part in determining the performance of the fan. The blade's geometry is an important design consideration for the flow separation at the blade surface and the stabilization of the flow pattern. Additionally, various studies have been carried out to improve the blade's function because it plays a decisive role in the overall performance, such as the internal flow and the efficiency, of the fan.

Wu et al. [1] proposed an optimal profile design method for centrifugal impeller blades by controlling their velocity distribution. Dou et al. [2] carried out numerical simulations on the flow of a plenum fan equipped with rotating vaneless diffusers with different diameter ratios and proposed the optimum diameter ratio according to the flow coefficient. Lee et al. [3] analyzed the effects of the bending length (ℓ/c) and the bending angle (θ) in the leading-edge direction on the impeller trailing edge of the centrifugal fan as design variables by numerical simulation. Park et al. [4] reviewed and studied the application of an airfoil impeller to improve the aerodynamic performance of a centrifugal fan in high-speed rotation. It was confirmed that the application of an airfoil impeller greatly reduced the flow separation that occurs on the blade pressure and diffuser pressure surfaces compared with the existing blade shape. Siwek et al. [5] presented the numerical model of the centrifugal fan and conducted experiments to verify the fan's performance characteristics. As a result, the accuracy of the numerical model was verified. Kim et al. [6] presented a numerical analysis model

for the splitter-type centrifugal fan and confirmed that the splitter blade improved the fan's overall performance. Chunxi et al. [7] conducted a study on the performance of centrifugal fans with 5% and 10% increases in the impeller size by extending the tip of the blade without changing the size of the volute. By extending the blade tip to increase the size of the impeller, the flow rate, voltage, and axial force of the fan increased during operation. However, although the nonuniformity of the flow in the volute increased, the overall efficiency of the fan decreased. Lin et al. [8] conducted a numerical analysis for flow visualization, torque calculation, efficiency, and noise for centrifugal fans with a small-diameter rear wing for computer cooling. Ni et al. [9] conducted numerical investigation by using ANSYS-Fluent on the internal flow of a Sirocco fan to investigate the effects of the inclination angle of the blades on the fan performance. The effects of the inclined blade are demonstrated by the variations in static pressure, efficiency, and pressure and velocity distributions at various inclination angles. Additionally, there have been numerical analyses and experimental studies on the method of reducing noise by changing the structure of the volute or the material of the volute tongue of the centrifugal blower [10–14]. However, there has been little research on improving the efficiency of scroll-less plenum blowers.

In this study, we optimized the airfoil blade of the plenum fan and compared its performance with that of the original model. Our optimally designed blade had four layers, and the iteration method was introduced to calculate the optimal design value of each layer.

2. Numerical Investigation

2.1. Numerical methods

The commercial CFD solver of ANSYS-CFX 17 [15] was used for the numerical analysis to evaluate the performance of the plenum fan. The fan's inlet and outlet were set to an open boundary condition, the inlet pressure was set to atmospheric pressure, and the wall condition was set to a no-slip wall condition. The impeller's rotation speed was set to 1,100 RPM, and the simulation was carried out based on the flow rate given in the product. The numerical calculations were discretized using three-dimensional, incompressible Reynolds Averaged Navier–Stokes (RANS) equations. The normal numerical analysis was carried using the pressure based on the fully coupled implicit method. The turbulence model uses a shear-stress transport model (SST), which is useful for the analysis of the flow separation.

Generally, in flow analysis using CFD, attention should be paid to y+ of the first grid point to analyze the boundary layer of the wall, and y+ should be 1–2 or less in the case of a low-Reynolds-number turbulence model, analyzing from the viscous sublayer of the wall. However, to satisfy these conditions, there are many grids densely packed on the wall surface, and thus, the total number of grids is greatly increased. To solve this, the wall function is usually used to reduce the number of grids concentrated on the wall. With the automatic wall function of CFX, if the first grid y+ is located between 1 and 100, the flow analysis results and the theoretical equations agree well with the grid y+ such that the y+ problem on the wall can be solved [16]. When analyzed using CFX, the flow analysis can be performed without worrying about the y+ by simply driving the grid on the wall such that the optimization results based on the flow analysis can be trusted.

2.2. Governing equations

The continuity equation and momentum equation applied in this study can be expressed in a conservation form as follows:

- Continuity equation:

$$\frac{\partial u_i}{\partial x_i} = 0 \quad (1)$$

where u_i is the instantaneous velocity in the i direction.

- Momentum equation:

$$\frac{\partial}{\partial t}(\rho u_i) + \frac{\partial}{\partial x_j}(\rho u_i u_j) = -\frac{\partial P}{\partial x_j} + \frac{\partial \tau_{ij}}{\partial x_j} \rho f_i \quad (2)$$

where P is the static pressure, τ_{ij} is the viscous stress tensor, and f_i is the body force.

In Newtonian fluids, τ_{ij} can be expressed in terms of the velocity gradients as shown in equation (3).

$$\tau_{ij} = \mu\left(\frac{\partial u_i}{\partial x_j} + \frac{\partial u_j}{\partial x_i}\right) - \frac{2}{3}\mu\left(\frac{\partial u_m}{\partial x_m}\right)\delta_{ij} \quad (3)$$

where μ is the fluid dynamic viscosity and δ_{ij} is the Kronecker delta.

Equation (2) and equation (3) can be used to obtain the Navier–Stokes equation of equation (4):

$$\frac{\partial}{\partial t}(\rho u_i) + \frac{\partial}{\partial x_j}(\rho u_i u_j) = -\frac{\partial P}{\partial x_j} + \frac{\partial}{\partial x_j}\left(\mu\left(\frac{\partial u_i}{\partial x_j} + \frac{\partial u_j}{\partial x_i}\right) - \frac{2}{3}\mu\left(\frac{\partial u_m}{\partial x_m}\right)\delta_{ij}\right) + \rho f_i \quad (4)$$

To simplify the problem, we used the method of averaging the Navier–Stokes equation. Equation (5) shows the Reynolds Averaged Navier–Stokes (RANS) equation:

$$\frac{\partial}{\partial t}(\overline{\rho u}_i) + \frac{\partial}{\partial x_j}(\overline{\rho u}_i \overline{u}_j) = -\frac{\partial \overline{P}}{\partial x_j} + \frac{\partial}{\partial x_j}\left(\overline{\mu}\left(\frac{\partial \overline{u}_i}{\partial x_j} + \frac{\partial \overline{u}_j}{\partial x_i}\right) - \frac{2}{3}\overline{\mu}\left(\frac{\partial \overline{u}_m}{\partial x_m}\right)\delta_{ij}\right) + \frac{\partial}{\partial x_j}\left(-\overline{\rho u_i' u_j'}\right) + \overline{\rho f_i} \quad (5)$$

2.3. Geometrical model and mesh

The original plenum fan model is PRL-560L0. The geometric shapes are shown in Figure 1, and the specifications are shown in Table 1. Figure 2 shows the computational domain. The radius of the computational domain was three times the diameter of the plenum fan, and the height was set to 30 times the width of the plenum fan. Block 1 is the area at which the flow enters through the bell mouse, and Block 2 is the fan part and the rotating flow area. Block 3 is the area where there is rotational flow. The flow field is treated as a wall. As a boundary condition, the inlet condition is the pressure inlet condition, the outlet condition is the mass flow rate condition, and the air density corresponds to 25°C. The size of the domain was considered large enough to avoid interference in the flow.

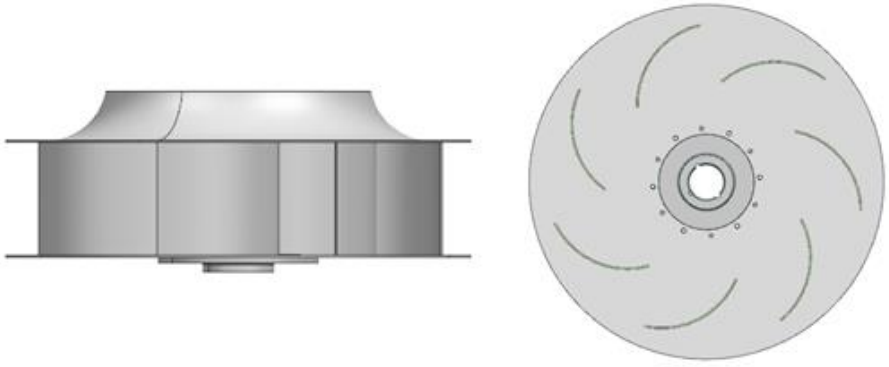

Figure 1. Geometric shape of the original model (PRL-560L0).

Table 1. Rated variables of the plenum fan.

Variables	Units	Value
Flow coefficient	-	0.675
Static pressure	Pa	392
Static pressure efficiency	%	71.8
Impeller diameter	mm	640
Impeller outlet breadth	mm	167
Number of blades	-	7
Revolving speed	rpm	1100

Figure 3 shows the axial cross-section of the original model's mesh system. Since the impeller and shrouds were curved and exhibited complex geometrical shapes, a high-quality structured grating could not be applied, so an unstructured grating was used. For analysis, 9.4 million gratings were constructed for the impeller and the bell mouth, and 7.4 million tetrahedra and 2 million wedges were applied.

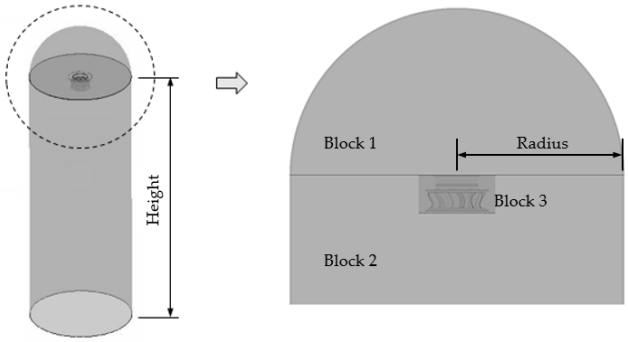

Figure 2. Computational domain.

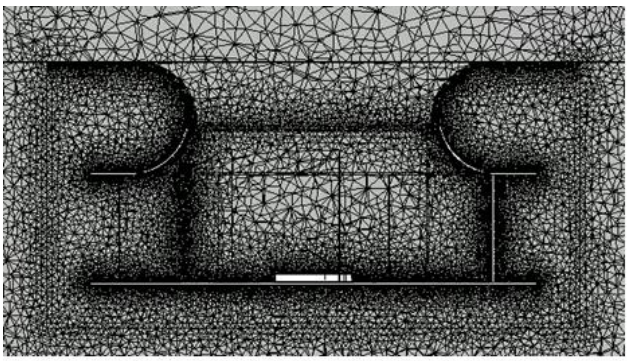

Figure 3. Mesh system.

2.4. Experimental results and comparison with the numerical simulation

To examine the validity of the original model's numerical results, the experimental results under the design conditions were compared with the numerical results. This is shown in Figure 4. It can be seen that the CFD results and the experimental results are in good agreement with the rated airflow rate and the static pressure conditions.

Preprints (www.preprints.org) | NOT PEER-REVIEWED | Posted: 17 April 2020 doi:10.20944/preprints202004.0295.v1

Peer-reviewed version available at Appl. Sci. 2020, 10, 3460; doi:10.3390/app10103460

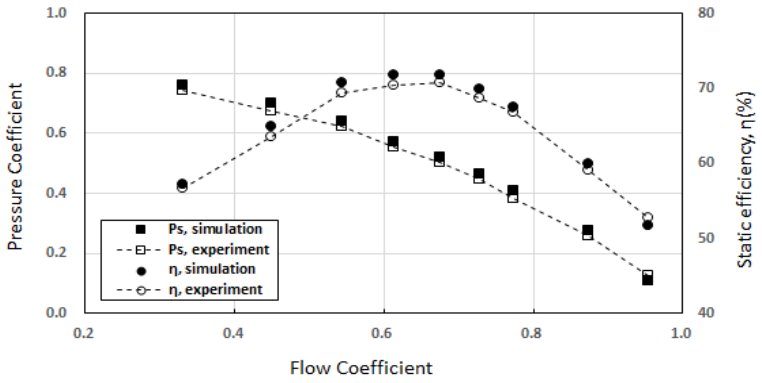

Figure 4. Comparison between the numerical and experimental results (@1,100 RPM).

3. Optimization of the Blade Profile

In this study, to design the optimum airfoil of the plenum fan, the blade was divided into four layers, and the optimum airfoil was designed for each layer. Figure 5 shows a three-dimensional curved shape and an image of the blade with four layers.

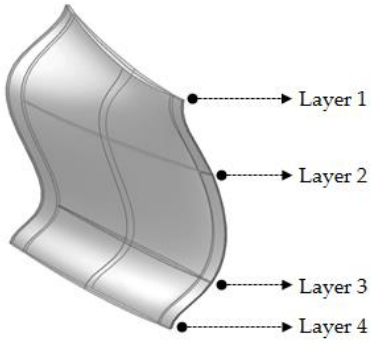

Figure 5. Layer definition of the plenum fan blade.

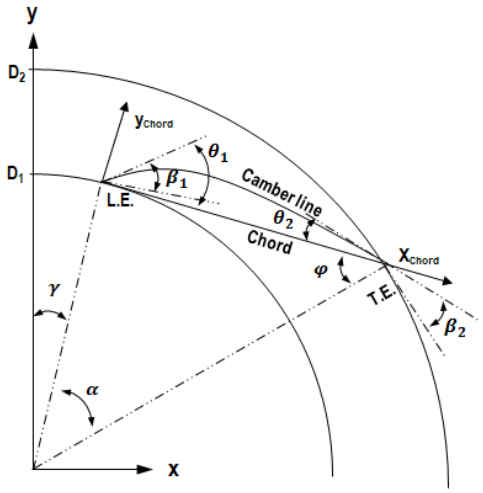

Figure 6. Airfoil design parameters.

The airfoil was designed using NACA four-digit. The basic design parameters required to design the airfoil are shown in Figure 6. D1 and D2 are the values that determine the radial positions of the leading and trailing edges and can be defined as the inner and outer diameters. γ, α, and β_1

Preprints (www.preprints.org) | NOT PEER-REVIEWED | Posted: 17 April 2020 doi:10.20944/preprints202004.0295.v1

Peer-reviewed version available at Appl. Sci. 2020, 10, 3460; doi:10.3390/app10103460

are all angles, where γ is the relative position of the airfoil's leading edge, α is the code angle corresponding to the airfoil length, and β_1 is the incidence angle. Note that when defining β_1, the minimum value of β_1 ($\beta_{1,min}$) is determined using D1, D2, and α. This value can be calculated using the following equations:

$$l_c = \sqrt{\left(\frac{D_1}{2}\right)^2 + \left(\frac{D_2}{2}\right)^2 - 2\frac{D_1}{2}\frac{D_2}{2}\cos(\alpha)} \tag{6}$$

$$2\frac{D_1}{2} l_c \cos\left(\beta_{1,min} + 90^\circ\right) = \left(\frac{D_1}{2}\right)^2 + l_c^2 - \left(\frac{D_2}{2}\right)^2 \tag{7}$$

$\theta_1, \theta_2, \varphi$ are defined using the geometric relationship as follows:

$$\varphi = \cos^{-1}\left[\frac{c^2 + \left(\frac{D_2}{2}\right)^2 - \left(\frac{D_1}{2}\right)^2}{2c\left(\frac{D_2}{2}\right)}\right] \tag{8}$$

$$\theta_1 = \alpha + \varphi - \left(\frac{\pi}{2} - \beta_1\right)$$

$$\theta_2 = \frac{\pi}{2} - \beta_2 - \varphi$$

The thickness distribution for the NACA four-digit section is selected to correspond closely to that for these wing sections and is given by

$$y_t = \frac{t}{0.2} c \left[0.2969\sqrt{\frac{x}{c}} - 0.1260\left(\frac{x}{c}\right) - 0.3516\left(\frac{x}{c}\right)^2 + 0.2843\left(\frac{x}{c}\right)^3 - 0.1015\left(\frac{x}{c}\right)^4\right] \tag{9}$$

where C is the code length, x is a position along the code from 0, y is half the thickness at the x position, and t is the maximum thickness.

In this study, the iteration method was introduced to optimally design the plenum fan with a three-dimensional blade. The flowchart of the iteration method used in the calculation is shown in Figure 7, and the Taguchi method is used for initial factor selection.

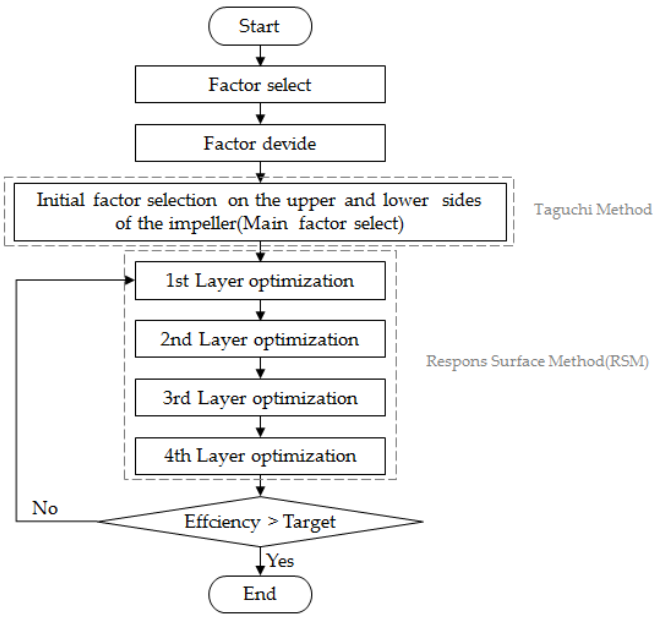

Figure 7. Flowchart of the iteration method for blade optimization.

Preprints (www.preprints.org) | NOT PEER-REVIEWED | Posted: 17 April 2020 doi:10.20944/preprints202004.0295.v1

Peer-reviewed version available at Appl. Sci. 2020, 10, 3460; doi:10.3390/app10103460

Layers 1, 4 and 2, 3's parameters were simultaneously considered to attain the initial values for each layer. Layer 1 was selected as the plane where the blade met the shroud and consisted of six design variables: α, γ, β_1, D1, D2, and height. Layer 4 was selected as the plane where the blade met the back plate. It consisted of five design variables: α, γ, β_1, D1, and D2. To select the major design variables, L12 analysis was used for 11 factors, and screening analysis was performed by computational simulation. The main effect analysis results of Layer 1 and Layer 4 are shown in Figure 8(a), and the effects of α at Layer 1 and D1, D2, and γ at Layer 4 are significant. The first optimization of Layers 1 and 4 was performed using the analysis of four factor-3 levels where selected as the main effect analysis using the response surface method (RSM).

In Layers 2 and 3, we selected an arbitrary cross-section of the blade, and these two layers consisted of six design variables such as α, γ, β_1, D1, D2, and height. To select the major design variables, L16 analysis was used for 12 factors, and screening analysis was performed by computational simulation. The main effect analysis results of Layer 2 and Layer 3 are shown in Figure 8(b), and the effects of γ at Layer 2 and γ, β_1, and D2 at Layer 3 are significant. A second optimization of Layers 2 and 3 was performed in the same way as that in the first optimization, and the values of Layers 1 and 4 were used to optimize the results from the first optimization.

After the first and second optimizations, the shape of the initial model could be determined. Once the initial shape was determined, the optimal design values were obtained from Layer 1 using the RSM. The iteration was performed by applying this value to the Layer 2 optimization. The calculations were repeated and finally converged to the target static pressure efficiency of 76% to complete the optimization. The optimal design values of the blades designed by the iteration method are shown in Table 2. The blade shapes of the original and optimized models are shown in Figure 9.

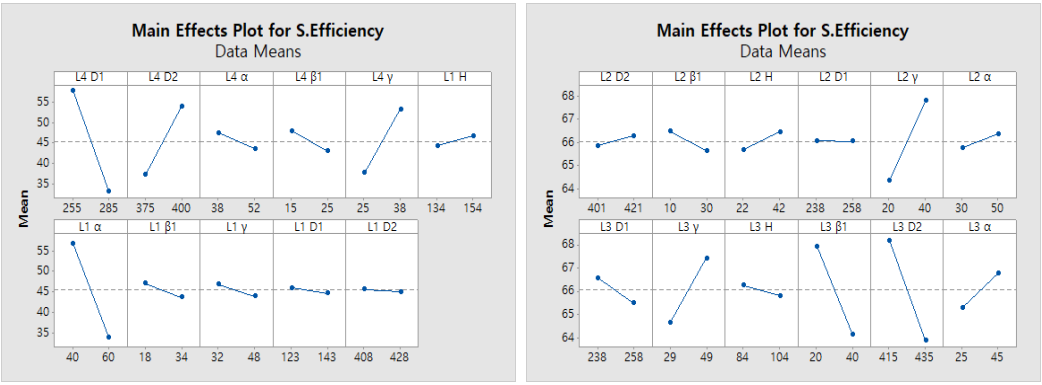

(a) (b)

Figure 8. Main effect plot of the airfoil parameters: (a) Layers 1 and 4 and (b) Layers 2 and 3.

Table 2. Design values after blade optimization.

Part	Parameters	Unit	Value	Part	Parameters	Unit	Value
Layer 1	D1	mm	340.0	Layer 3	D1	mm	330.0
	D2	mm	475.0		D2	mm	527.0
	α	degrees	42.5		α	degrees	45.0
	β_1	degrees	6.4		β_1	degrees	30.6
Layer 2	D1	mm	298.0		H	mm	130.0
	D2	mm	444.0	Layer 4	D1	mm	343.0
	α	degrees	47.5		D2	mm	478.0
	β_1	degrees	6.8		α	degrees	45.0
	H	mm	42.0		β_1	degrees	15.0

Preprints (www.preprints.org) | NOT PEER-REVIEWED | Posted: 17 April 2020 doi:10.20944/preprints202004.0295.v1

Peer-reviewed version available at Appl. Sci. 2020, 10, 3460; doi:10.3390/app10103460

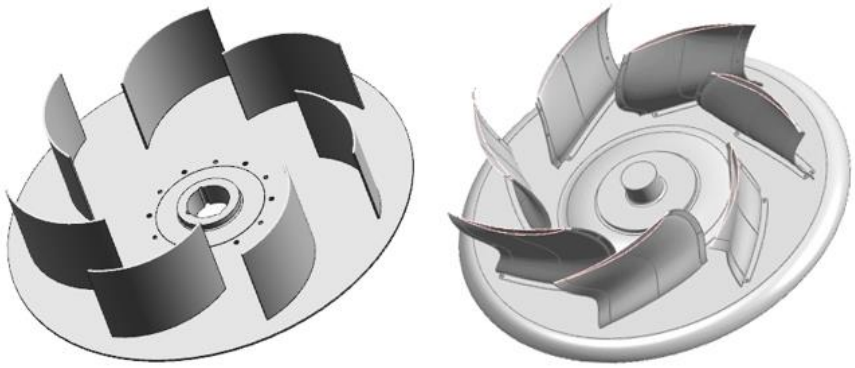

(a) (b)

Figure 9. Geometric shape of the blades of the original and optimized models: (a) Original model and (b) Optimized model.

4. Numerical Results and Discussion

4.1. Mesh independence verification

Table 3 shows the mesh independence verification results of the optimized model. When the total elements are beyond 9,461,970, the change in static pressure is small.

Table 3. Mesh independence verification of the optimized model.

No.	Mesh	Static pressure [Pa]
1	7,432,111	418
2	8,184,320	415
3	8,954,841	410
4	9,461,970	398
5	9,806,594	397

4.2. Comparison of the performances of the original and optimized models

Figure 10 shows the performance comparison between the original model and the optimized model. Both the static pressure and the static efficiency of the optimized model were improved compared with those of the original model. The highest efficiency of the optimized model was 78.1% at the point with a flow coefficient of 0.675, which was an improvement of more than 6% compared with that of the original model. Figure 11 shows the static pressure distribution in the middle section of the original and optimized models. In the optimized model, the static pressure in the channel increased uniformly and stably. By contrast, the original model showed a relatively large loss at the blade outlet.

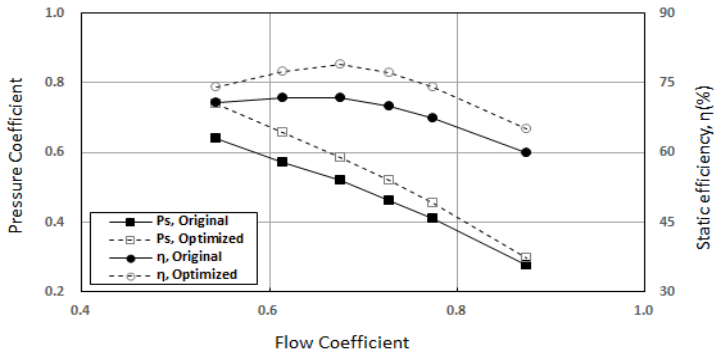

Figure 10. Comparison of performances between the original and optimized models (@1,100 RPM).

Figure 12 shows the relative velocity distributions in the middle section of the original and optimized models. A low-velocity region occurs on the suction surface of the original model, and a high-velocity region occurs on the blade's outlet surface. In the optimized model, the homogeneous velocity distributions on the suction surface and the channel can be observed. The inhomogeneous velocity distribution on the suction surface or outlet surface is the main cause of flow separation, which causes fluid flow friction, resulting in large losses and performance degradation.

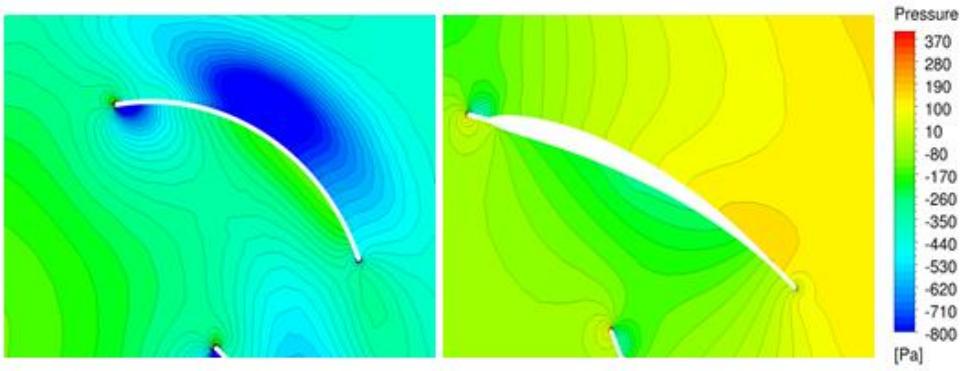

(a) (b)

Figure 11. Static pressure distribution (@1,100 RPM): (a) Original model and (b) Optimized model.

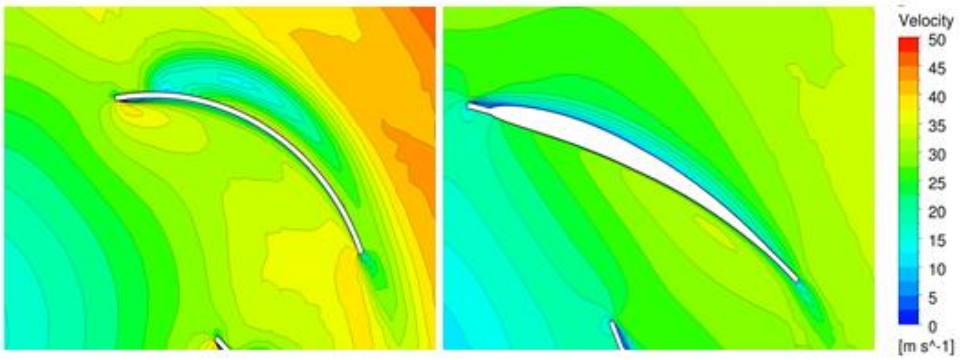

(a) (b)

Figure 12. Velocity distribution (@1,100 RPM): (a) Original model and (b) Optimized model.

Figure 13 shows the velocity streamline at the blade and the channel. In the original model, the fluid flow on the suction and outlet surfaces does not flow along the blade airfoil, and separation occurs. In the optimized model, on the other hand, some flow separation occurs at the blade tip, but the overall flow is stable along the blade airfoil. This stable flow reduces the fluid flow friction in the impeller to increase the performance and reduce noise.

Figure 14 shows the turbulence eddy frequencies of the original and optimized models. In the original model, turbulence increases because of flow separation from the leading edge. On the other hand, in the optimized model, the flow separation at the leading edge is significantly reduced, making the flow stable. Additionally, the loss in the impeller outlet is significantly reduced in the optimized model. As a result, uniform and stable control of the flow in the blade can be seen as a major factor in increasing the efficiency of the plenum fan.

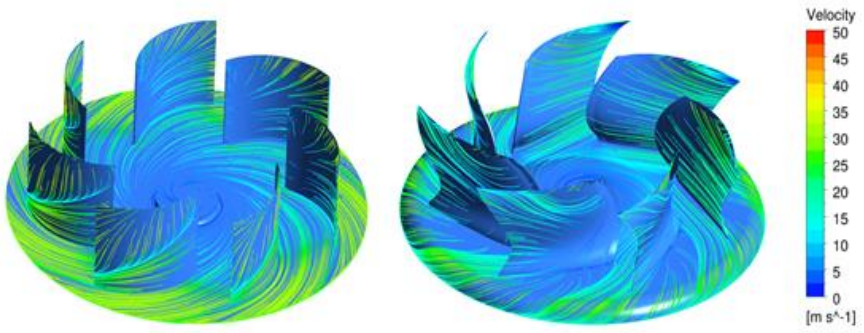

(a) (b)

Figure 13. Velocity streamline on the surface (@1,100 RPM): (a) Original model and (b) Optimized model.

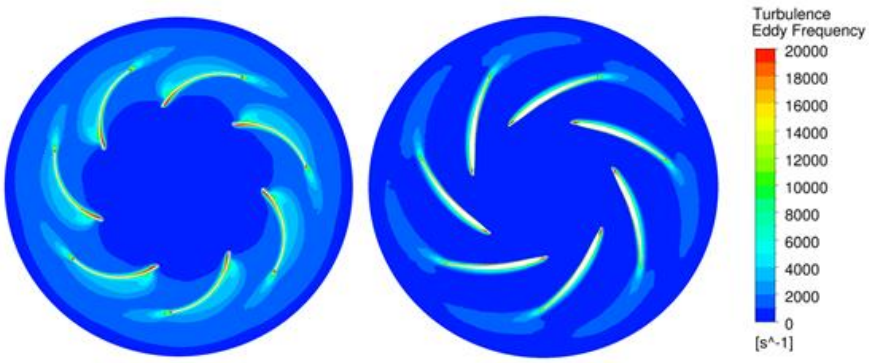

(a) (b)

Figure 14. Turbulence eddy frequency (@1,100 RPM): (a) Original model and (b) Optimized model.

5. Conclusions

In this study, we optimized the performance of a plenum fan with a four-layer three-dimensional blade. The numerical calculations of the original and optimized models were based on the three-dimensional and incompressible RANS equation. The SST model, which is useful for the analysis of flow separation, was used for the turbulence model. The numerical results of the original model are in good agreement with the experimental results. The summarized conclusion is as follows.

1. The smooth, curved surface of the three-dimensional blade of the optimized model stabilized the flow and reduced the flow friction by restraining the flow separation as much as possible. The results show that both static pressure and static efficiency were improved in the optimized model compared with the original model. The static efficiency of the optimized model was improved by more than 6% compared with that of the original model at its peak.

2. In the original model, a relatively large loss occurred at the blade outlet. Additionally, in the original model, it was confirmed that turbulence grows because of flow separation from the leading edge. However, in the optimized model, the static pressure in the channel increased uniformly and stably. The flow separation at the leading edge was significantly reduced, which made the flow stable.

Author Contributions: Y.C.A. provided the basic idea for this study and administrated the project. K.J.L. provided numerical strategies, basic concept of optimization and worked on the analysis of numerical results. Y.M.K. carried out the numerical simulations. I.W.P. and K.S.B. carried out the experiments and comparison with simulation results

Funding: ----

Acknowledgments: This work was supported by the National Research Foundation of Korea(NRF) grant funded by the Korea government(MSIT) (No. 2018R1A2B6004137)

Conflicts of Interest: The authors declare no conflict of interest.

References

1. Wu, L.; Dou, H.; Wei, Y.; Chen, Y.; Cao, W.; Ying, C. Optimization of blade profile of a plenum fan. *Internal Journal of Fluid Machinery and Systems*, 2016, January-March, 9, No.1, 95-106.
2. Dou, H.; Wu, L; Wek, Y.; Chen, Y.; Cao, Ying, C. Employing rotating vaneless diffuser to enhance the performance of plenum fan. *Internal Journal of Fluid Machinery and Systems*. 2017, January-March, 10, No.1, 9-18.
3. Lee, J.; Jeon, H.; Jang, C. Performance characteristics according to the outlet impeller blade shape of a centrifugal blower. *The KSFM Journal of Fluid Machinery*. 2013, 16, 12-18.
4. Park, K.; Park, C. Application of airfoil impeller for enhancement of aerodynamic performance of high speed centrifugal fan. *Trans. Korean Soc. Mech. Eng*. 2016, B, 40, 321-327.
5. Siwek, T.; Gorski, J.; Fortuna S. Numerical and experimental study of centrifugal fan flow structures and their relationship with machine efficiency. *Pol. J. Environ. Stud*. 2014, 23, No. 6, 2359-2364.
6. Kim, J.; Cha, K.; Kim, K.; Jang, C. Numerical investigation on aerodynamic performance of a centrifugal fan with splitter blades, *International Journal of Fluid Machinery and Systems*. 2012, 5, No. 4, 168-173.
7. Li Chunxi, Wang Song Ling, Jia Yakui, 2012, "The performance of a centrifugal fan with enlarged impeller", Energy Conversion and management, 52, pp. 2902-2910
8. Lin, S.; Tsai, M. An integrated performance analysis for a backward-inclined centrifugal fan. *Computers and Fluids*. 2012, 56, 24-38.
9. Ni, S.; Cao, W.; Xu, J.; Wang, Y.; Zhang W. Effects of an inclined blade on the performance of a sirocco fan. *Appl. Sci*. 2019, 9, 3154-3176
10. Xu, C.; Mao, Y. Experimental investigation of metal foam for controlling centrifugal fan noise. *Applied Acoustics*. 2016. 104. 182-192.
11. Baloni, B.; Pathak Y.; Channiwala S. Centrifugal blower volute optimization based on Taguchi method. *Computers & Fluids*. 2015. 112. 72-78.
12. Heo, S.; Cheong, C.; Kim, T. Development of low-noise centrifugal fans for a refrigerator using inclined S-shaped trailing edge. *Internal Journal of Refrigeration*. 2011. 34. 2076-2091.
13. Park, S.; Ryu, S.; Cheong, C.; Kim, J.; Park, B.; Ahn Y.; Oh, S. Optimization of the orifice shape of cooling fan units for high flow rate and low-level noise in outdoor air conditioning units. *Appl. Sci*. 2019, 9, 5207-5223
14. Zhang, J.; Chu, W.; Yi, L. Vibroacoustic optimization study for the volute casing of a centrifugal fan. *Appl. Sci*. 2019, 9, 859-891
15. ANSYS CFX 17.0, ANSYS CFX Tutorials, 2016, ANSYS Inc.
16. Menter, F.R., Two-Equation Eddy-Viscosity turbulence models for engineering applications. *AIAA-Journal*. 1994. 32. 269-289.